

Fast detection and low power hydrogen sensor using edge-oriented vertically aligned 3-D network of MoS₂ flakes at room temperature

A. V. Agrawal,¹ R. Kumar,² S. Venkatesan,³ A. Zakhidov,³ Z. Zhu,⁴ Jiming Bao,⁴ Mahesh Kumar,² and Mukesh Kumar^{1,a)}

¹Functional and Renewable Energy Materials Laboratory, Indian Institute of Technology Ropar, Punjab 140001, India

²Department of Electrical Engineering, Indian Institute of Technology Jodhpur, Jodhpur 342011, India

³Department of Physics, Texas State University, San Marcos, Texas 78666, USA

⁴Department of Electrical and Computer Engineering, University of Houston, Houston, Texas 77204, USA

(Received 3 May 2017; accepted 15 August 2017; published online 29 August 2017)

The increased usage of hydrogen as a next generation clean fuel strongly demands the parallel development of room temperature and low power hydrogen sensors for their safety operation. In this work, we report strong evidence for preferential hydrogen adsorption at edge-sites in an edge oriented vertically aligned 3-D network of MoS₂ flakes at room temperature. The vertically aligned edge-oriented MoS₂ flakes were synthesised by a modified CVD process on a SiO₂/Si substrate and confirmed by Scanning Electron Microscopy. Raman spectroscopy and PL spectroscopy reveal the signature of few-layer MoS₂ flakes in the sample. The sensor's performance was tested from room temperature to 150 °C for 1% hydrogen concentration. The device shows a fast response of 14.3 s even at room temperature. The sensitivity of the device strongly depends on temperature and increases from ~1% to ~11% as temperature increases. A detail hydrogen sensing mechanism was proposed based on the preferential hydrogen adsorption at MoS₂ edge sites. The proposed gas sensing mechanism was verified by depositing ~2–3 nm of ZnO on top of the MoS₂ flakes that partially passivated the edge sites. We found a decrease in the relative response of MoS₂-ZnO hybrid structures. This study provides a strong experimental evidence for the role of MoS₂ edge-sites in the fast hydrogen sensing and a step closer towards room temperature, low power (0.3 mW), hydrogen sensor development. *Published by AIP Publishing.* [<http://dx.doi.org/10.1063/1.5000825>]

Hydrogen is the efficient source of energy and produces zero pollution when burned with oxygen or air.¹ Oxidation of hydrogen forms water as a side product, and an enormous amount of clean energy is generated. This energy is being widely used in space and civil transport. Nonetheless, hydrogen is explosive in nature when mixed with air even in a small concentration (~4%).² Hence, fast detection of hydrogen gas well below the critical concentration is very crucial for the safety purpose of next generation clean energy production and regulation.

Recently, 2-D MoS₂, a transition metal dichalcogenide (TMDC), has shown potential for various optical, electronic, and gas sensing applications due to their inborn direct band gap which allows better control over the carriers in contrast to other 2-D materials including graphene.³ Monolayer MoS₂, ~0.65 nm thick, has the direct band gap of ~1.8 eV, while the band gap is decreased down to 1.2 eV and shifted to the indirect band gap as the number of layers increased.⁴ The semiconducting nature of MoS₂ opens its applications in many areas such as optoelectronics,⁵ solar cells,⁶ water disinfection with visible light,⁷ nanoelectronic devices,⁸ and catalysis activities.⁹

Furthermore, atomically thin 2-D MoS₂ showed its potential for gas sensing applications.^{10,11} Either MoS₂ nanocomposites (MoS₂-Pd) or MoS₂ heterostructures (Pt-MoS₂/MoO₃) were utilized for hydrogen detection.^{12–14} In these reports, the sensitivity ($\Delta R/R$) of a bare MoS₂ sensor to hydrogen exposure was observed to be negligible, while high

sensitivity and slow response for MoS₂ nanocomposites and MoS₂/Si heterostructures were observed. In most of these studies, basal plane MoS₂ is used for gas sensing applications which is considered, thermodynamically, to be more inert than the edge sites in MoS₂.^{15,16} Recently, researches focused on the growth of vertically aligned MoS₂^{17,18} with its edge sites perpendicular to the substrate plane and explored for hydrogen evolution reaction and for other enhanced catalytically activities.^{18,19} It was observed that the edge sites of MoS₂ are much more reactive than the terrace of the basal plane MoS₂.¹⁶ Hence, gas adsorption may greatly be augmented by the vertically aligned MoS₂ films. However, there is no report in the literature especially on the highly reactive and exposed edges of MoS₂ for hydrogen detection applications.^{12–14}

In this paper, we present H₂ gas sensing for an edge-oriented 3-D network of vertically aligned MoS₂ flakes. The effect of different operating temperatures (28–150 °C) on the sensitivity, response time, and recovery time is studied with 1% concentration of hydrogen, which is well below the explosive limit of hydrogen in ambient. The overall response time in the range of 14.3 s to 20.4 s is observed. To confirm the role of MoS₂ edges for hydrogen sensing, a thin ZnO film (2–3 nm) was deposited on MoS₂ flakes, and the sensor response was studied for MoS₂-ZnO hybrid structures. It is found that the sensor response decreased nearly 50% due to partial passivation of favorable sites for hydrogen adsorption in MoS₂ flakes. This study clearly revealed the role of edge sites for preferential hydrogen adsorption and its fast detection.

^{a)}Author to whom correspondence should be addressed: mkumar@iitrpr.ac.in

MoS₂ edge-oriented vertically aligned flakes were synthesized on a Si/SiO₂ substrate via a modified *tube-in-tube* CVD process. For more details, see the [supplementary material](#). In brief, high purity MoO₃ (99.97%, Sigma Aldrich) and sulfur powder (99.98%, Sigma Aldrich) were used for the growth of MoS₂ flakes. The cleaned substrate was placed on the top of MoO₃ powder boat. The small tube with one end closed loaded with powders, and the substrate was placed inside a bigger quartz tube in such a way that the close end faced the gas inlet (see Fig. S1 in the [supplementary material](#)). Ar gas flow was maintained at 225 sccm throughout the deposition. The close end of the small tube was in zone 1 (MoO₃), and the open end was in zone 2 (S). The growth temperature for zone 1 and zone 2 was fixed at 800 °C and 350 °C, respectively (see Fig. S1 in the [supplementary material](#)). The growth time was 30 min followed by cooling to RT at the same Ar flow.

The surface morphology of as-grown MoS₂ flakes was studied using a FEI Helios Nano Lab 400 with a probe current of 0.34 nA and an accelerating voltage of 10 kV. Raman and photoluminescence (PL) were done using a HORIBA IHR320 spectrometer. A 532 nm laser was used as the excitation source with a power of 500 μW to avoid any heating effect on the samples. Metal contacts in the shape of circular dots of Au/Cr having a thickness 250/3–5 nm with 100 μm diameter were deposited through physical mask by thermal evaporation. The separation between the two metal dots was ~100 μm. The gas sensor response was measured with 1% hydrogen concentration diluted with 99% argon in a home-build gas sensing system equipped with a mass flow controller and a proportional–integral–derivative (PID) controlled heater for accurate measurements. The sensing measurement was done in the operating temperature range of 28–150 °C using a computer controlled Keithley 4200.

Figure 1(a) shows the field emission-scanning electron microscopy (FE-SEM) images of as-grown MoS₂ flakes. The results clearly indicate that these flakes are vertically grown from the substrate and interconnected to each other and form an interconnected 3-D network. The dotted line in Fig. 1(a) is the guide to the eye for MoS₂ interconnection from one end to another end. The inset shows the high magnified FE-SEM image of flakes. The thickness of typical MoS₂ flakes, as shown in the high magnified FE-SEM image, is ~1.5 nm, which confirms that MoS₂ flakes are few-layered in nature. The Raman spectrum of edge-oriented MoS₂ flakes is shown in Fig. 1(b). Three coincide spectra of the Raman signal from three different areas are observed and showed the uniformity of the few-layer MoS₂ films. Two Raman modes are active at Raman absorbed wavenumbers of 384.90 cm⁻¹ and 410.05 cm⁻¹ which are attributed to E_{2g}¹ (*in-plane* mode) and A_{1g}¹ (*out-of-plane* mode) modes of MoS₂, respectively, as shown in Fig. 1(b).²⁰

The wave number difference between the E_{2g}¹ and A_{1g} modes is 25.15 cm⁻¹, which shows that MoS₂ has a few-layered structure which is also confirmed by FE-SEM analysis.²⁰ The PL spectra of these edge-oriented MoS₂ flakes were also recorded and are shown in the [supplementary material](#) (Fig. S2). Two peaks corresponding to A and B excitons are observed in the energy range of 1.82 eV–1.95 eV. This is in good agreement with the previous report for the few-layered MoS₂ structure.²¹

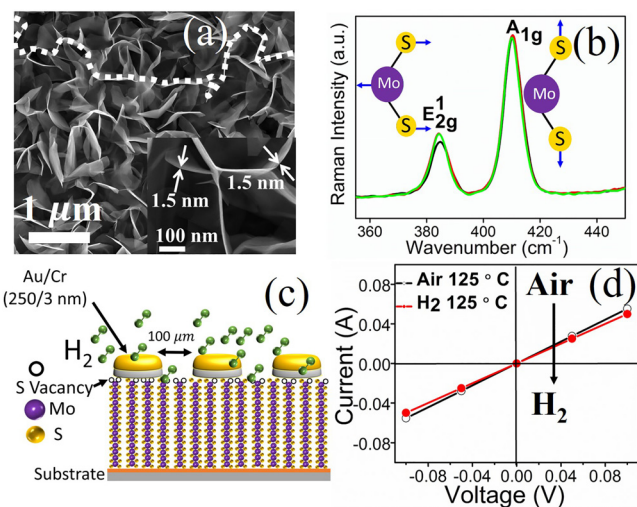


FIG. 1. (a) FE-SEM images of edge-oriented MoS₂ flakes show interconnected MoS₂ flakes that form a 3-D network. The inset shows a high magnification FE-SEM image. The thickness of the flake is ~1.5 nm, which indicates their few layered nature. (b) Raman spectrum taken at three different areas. Two active Raman modes E_{2g}¹ (*in-plane* vibration) and A_{1g}¹ (*out-of-plane* vibration) correspond to MoS₂. (c) 3-D Schematic diagram of an edge-oriented MoS₂ vertically aligned flake based hydrogen gas sensing device. (d) I-V characteristic curve obtained from the device at 125 °C in the presence of air and 1% hydrogen.

Finally, the edge-oriented MoS₂ flakes were tested for 1% hydrogen detection at different temperatures. The gas adsorption behavior of MoS₂ flakes is determined by the variation in the resistance at different operating temperatures (28–150 °C). We measured the resistance of the film by two-probe method with the Au/Cr contacts made on top of the MoS₂ flakes. Figure 1(c) shows the 3-D schematic of the hydrogen gas sensing device, and Fig. 1(d) shows the I-V characteristics of the device at 125 °C with and without hydrogen gas exposure. The exposed area between the two contacts was responsible for the gas sensing behavior of interconnected MoS₂ flakes. I-V characteristics clearly show that with the hydrogen exposure, the current is decreased and linear in nature. MoS₂ flakes are n-type in nature, and a decrease in the current implies that the hydrogen gas sensing takes the electron from the n-type MoS₂ flakes. So, as the hydrogen gas is exposed to the MoS₂ flakes, it increases the resistance between the two contacts by taking the electrons from the film, and thus, there is decrease in the current. I-V characteristics of the MoS₂ sensor are linear in nature for all temperatures with and without hydrogen exposure. Linear characteristics of the I-V curve also reliable from the matching work function of metal contact (5.1 eV) and MoS₂ flakes (4.2–5.2 eV).^{22,23} In our case, I-V characteristics of the MoS₂ sensor is linear in nature for all temperatures with and without hydrogen exposure, and this may be due to the matching work function of metal contact (5.1 eV) and MoS₂ flakes (4.2–5.2 eV).^{22,23} We have also calculated the maximum power consumption for the MoS₂ based hydrogen sensor, and we observed the lowest power consumption of 0.3 mW in comparison to the literature.^{24,25}

Figure 2(a) shows the change in sensitivity ((R_{Hydrogen} - R_{Air})/R_{Air}) of the MoS₂ sensor with temperature. The figure clearly shows that the resistance and hence the sensitivity of the sensor increase with hydrogen exposure. As the sensing}

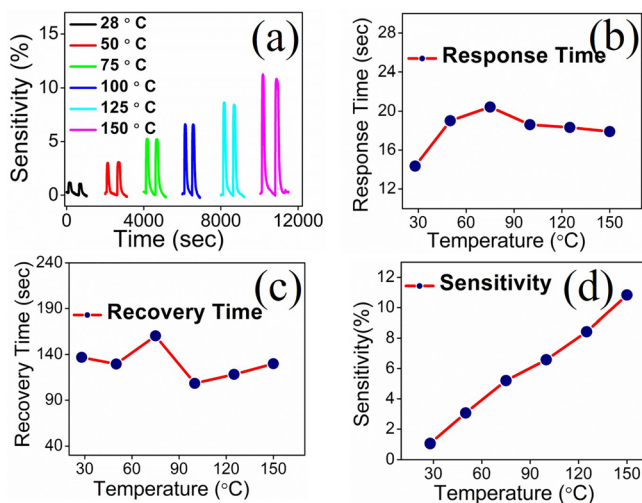


FIG. 2. (a) Sensitivity (%) vs time profile at different temperature (28–150 °C) with 1% concentration of hydrogen. (b) and (c) Response and recovery time curve. (d) Sensitivity (%) with temperature.

temperature increases from room temperature to 150 °C, the sensitivity increases from $\sim 1\%$ to $\sim 11\%$. The response and recovery time of the edge-oriented MoS₂ vertically aligned flakes are also plotted in Figs. 2(b) and 2(c), respectively. In the temperature range of 28–150 °C, the response time has changed from 14.3 s to 20.4 s. The observed overall response time is much lower than that for the other reported MoS₂ based hydrogen sensors.^{12–14} In a high operating temperature range (100–150 °C), the response time reaches a nearly saturated value around 18 s. The recovery time of the sensor is in the range of 108.3 s to 160.4 s. In a high-temperature range (100–150 °C), the device recovery time varies from 108 s to 129 s, which shows that the desorption rate of hydrogen at high temperature is nearly constant. Figure 2(d) shows the variation of sensitivity with temperature. It shows that sensitivity increases linearly up to 11% with temperature. The cyclability and stability of the sensor are tested for nearly 40 cycles and revealed almost the same sensitivity with a little change of $\pm 5\%$ for all the temperatures, which clearly signifies that the passivation of edge defects with hydrogen exposure is reversible in nature.

Table I summarizes the characteristics of the hydrogen sensor based on the MoS₂ flakes, MoS₂ composites and other nanostructures reported in the literature along with sensor characteristics in the present work. In all these reports, the hydrogen sensor made of edge-oriented MoS₂ flakes from this work shows the least or comparable response time for the fast detection of hydrogen at RT.

To understand the gas sensing behaviors for edge expose MoS₂ flakes, we consider the preferential interaction of hydrogen molecules with MoS₂ flakes. It is reported that thermodynamics favor to grow a basal plane as inert in comparison to the edge sites in MoS₂ flakes.¹⁶ The more defective nature of as grown edges in MoS₂ flakes is being utilized to enhance their catalytic activities.^{15,16} Here, it is observed that MoS₂ flakes are highly conducting in nature at all operating temperatures. This behavior can be attributed to the formation of favorable S vacancy at the edges which may be created during the synthesis of MoS₂ flakes. It is important to note that the energy required to remove the S atom and Mo atom from the MoS₂ layer is reported to be 6.1 eV and 13.9 eV,²⁹ respectively. So, the formation of S vacancies is more favorable during the growth. The S vacancy at the edges makes MoS₂ flakes as Mo-rich and responsible for their metallic like behavior.³⁰ In the 3-D interconnected network of MoS₂ layer structures, edges of MoS₂ behave as one-dimensional metallic wires due to the presence of localized metallic states,¹⁵ which is schematically shown as yellow lines in Fig. 3(a).

Position dependent adsorption of hydrogen molecules on MoS₂ was studied by the first principle calculations. Hydrogen molecule adsorption is determined by the negative adsorption energy, and hence, the most stable adsorption configuration on MoS₂ flakes for hydrogen gas is theoretically calculated.^{31,32} The adsorption energy is determined by $E_a = E_{\text{MoS}_2 + \text{molecule}} - (E_{\text{MoS}_2} + E_{\text{molecule}})$, where $E_{\text{MoS}_2 + \text{molecule}}$ is the net energy of MoS₂ and the adsorbed gas molecule and E_{MoS_2} and E_{molecule} are the total energy of MoS₂ and the single gas molecule. Negative adsorption energy means that the process is exothermic, and gas molecules have a strong interaction with MoS₂. Among the four available adsorption sites in MoS₂ [top of hexagon (H), top of Mo atoms (T_M), top of S atoms (T_S), and top of Mo-S bonds (B)], as shown in Fig. 3(b), the T_M sites have the adsorption energy of -82meV , H sites have the adsorption energy of -70meV , while T_S sites have the adsorption energy of -49meV .³² A similar trend in adsorption energy for hydrogen molecules at different sites in MoS₂ with a higher value for the T_M site (-131.61meV) was also observed in another report.³¹ Therefore, the hydrogen molecule has the highest probability to adsorb at Mo atom sites. It may be a non-zero probability for hydrogen gas adsorption at inert basal planes. However, in our case, the probability of interacting hydrogen at edges is much higher than the basal plane because of their defective nature. The calculated charge transfer from MoS₂ to the hydrogen molecule to be $0.05e$ ³¹

TABLE I. Reported literature on MoS₂ based hydrogen gas sensors and comparison with present work.

Material	Response time (s)	Recovery time (s)	Sensitivity (%)	Temp (°C)	References
MoS ₂ - Pd composites	40	83	10	RT	12
MoS ₂ /Si heterojunction	105	443.5 s	1.1×10^4	RT	13
Vertically aligned MoS ₂ /Si	108.7	101.9	685.7	RT	14
MoS ₂ functionalized by Pd	786	902	35.3	RT	26
MoO ₃ nano ribbons/graphene composite	10	30	20	RT	27
ZnO vertical nanorods	130	22	4000	250	28
Edge-oriented MoS ₂ flakes	14.3	136.85	1	RT	Present work

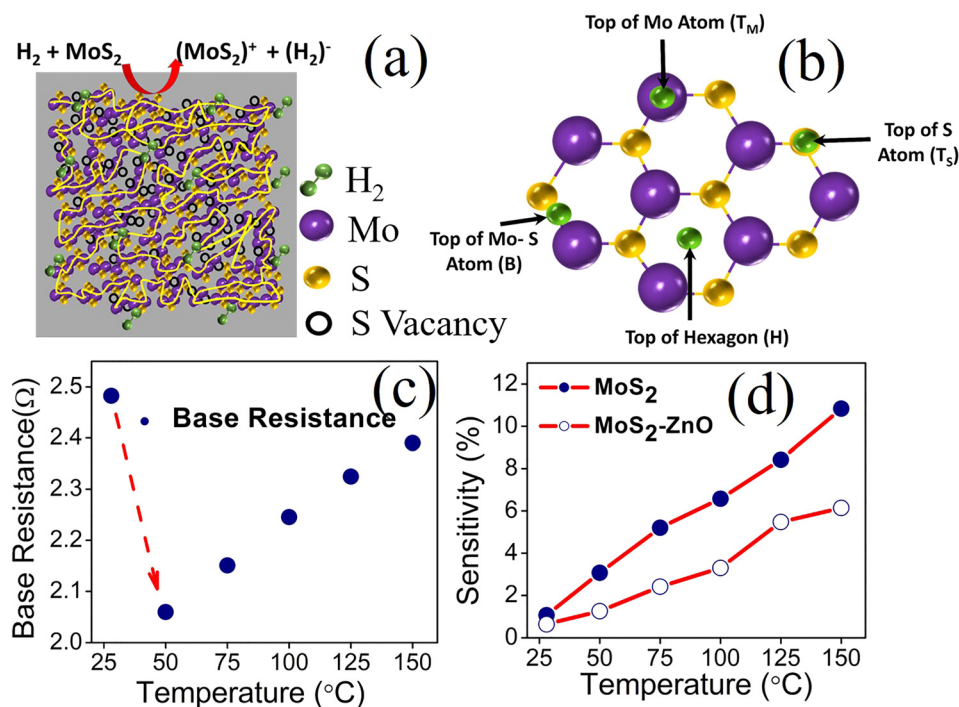


FIG. 3. (a). Top view of the edge oriented 3-D network of MoS₂ flakes. The yellow line shows the interconnected nature of metallic edges. The interacting hydrogen molecule is adsorbed by the MoS₂ edges and takes the electron from the film. (b) Top view of the favorable site for the hydrogen adsorption (c) Base resistance in the absence of hydrogen gas at different temperatures. (d) Sensitivity (%) vs temperature profile of bare MoS₂ and MoS₂-ZnO hybrid structures.

and $0.004e$,³² respectively, which implies that hydrogen plays as an electron acceptor.

From the above details, it is clear that hydrogen adsorption is most favorable along the edges of MoS₂ flakes rather than the basal plane and hydrogen behaves as the electron acceptor in nature for intrinsic n-type MoS₂.^{33,34} The edges of MoS₂ behave like metallic inter-connecting wires,¹⁵ and at room temperature, hydrogen is easily adsorbed. This increases the charge transfer of the MoS₂ flakes with exposed hydrogen gas at a much faster rate than the basal plane MoS₂. Thus, at room temperature, the device shows a very fast response time.

To understand the temperature dependent increase in sensitivity, we closely observed I-V characteristics and the resistance of the sensing device, with temperature in the absence of hydrogen. As the sensing temperature increases from 28 to 50 °C, the base resistance decreases dramatically as shown in Fig. 3(c). At room temperature, the device shows the higher base resistance of around 2.48 Ω, and then, it decreases to a minimum value of 2.05 Ω as the temperature increases from 28 °C to 50 °C. After 50 °C, the base resistance increases linearly with an increase in the temperature. This sharp decrease in the base resistance can be understood on the basis of the oxygen desorption from S vacancy sites in MoS₂ edges.

The oxygen adsorption plays a crucial role in inducing the doping effect in MoS₂ due to charge transfer.³⁵ The role of oxygen on MoS₂ and at the S vacancy sites was studied previously.³⁶ The first principles calculations were performed to calculate the binding energy of the oxygen molecule at defect free MoS₂ planes and at S vacancy sites in MoS₂ and the charge transfer to the adsorbed oxygen at these sites. The calculated binding energies between MoS₂ and S vacancy sites for adsorbed oxygen were found to be 0.102 eV and 2.395 eV, which clearly indicate the physical adsorption and chemically adsorption nature of oxygen at

two different sites, respectively. The calculated charge transfer between physically adsorbed oxygen to MoS₂ was $0.021e$, while chemically adsorbed oxygen at the S vacancies was higher, which is $0.997e$.

Thus, adsorbed oxygen bound at the S vacancies takes much more electrons than from MoS₂ flakes. Hence, at room temperature, adsorbed oxygen increased the resistance of the edge oriented MoS₂ flakes. Therefore, the base resistance in the absence of hydrogen gas at room temperature is higher than the other operating temperature as shown in Fig. 3(c). However, as the temperature increased from room temperature to 50 °C, the vacuum and heating simultaneously helped to remove the ambient oxygen from the flakes.³⁷ This leads to a fast decrease in the base resistance of the sensor with different temperatures and reaches a nearly intrinsic value as compared to room temperature even in the absence of hydrogen gas. With a further increase in the temperature, from 50 °C to 150 °C, the base resistance increases linearly, which may be due to the scattering of carriers in metallic like edges in MoS₂ flakes. The desorption of the O₂ molecule creates fresh active and favorable S vacancy sites for the adsorption of H₂ molecules. Hence, the film shows linearly increased sensitivity with temperature, and this phenomenon is continued as we further increased the temperature up to 150 °C.

To validate the proposed hypothesis and further understand the role of availability of favorable sites for hydrogen sensing, we deposited the 2–3 nm thin ZnO film using the RF magnetron sputtering technique on MoS₂ flakes and formed a hybrid structure of MoS₂-ZnO. The deposited ZnO film is not very thick to completely cover the MoS₂ flakes. It can partially passivate the edges of the MoS₂ flakes. Since MoS₂ flakes are vertically aligned, the probability to deposit ZnO on the edges is high. Thus, the number of favorable sites for the hydrogen adsorption may be reduced. The sensor response of MoS₂-ZnO hybrid structures was measured from room temperature to 150 °C for 1% hydrogen under identical

conditions. The sensitivity of the MoS₂-ZnO hybrid is shown in Fig. 3(d). The results revealed that sensitivity is nearly the same at room temperature, while it is reduced at a higher temperature. The decrease in the sensitivity of MoS₂-ZnO hybrid structures is the clear indication of the partial passivation of MoS₂ edge defect sites and decrease in sensitivity up to 50%, shown in Fig. 3(d). This provides strong experimental evidence of MoS₂ edge sites for hydrogen gas sensing applications.

In conclusion, we fabricated a 3-D network of edge-oriented vertically aligned MoS₂ flakes on a SiO₂/Si substrate via a modified *tube-in-tube* chemical vapor technique. Raman, PL, and FE-SEM results confirm that the synthesized flakes are edge oriented vertically aligned and few layered in nature. The response of this MoS₂ interconnected network was tested for 1% hydrogen in the operating temperature range of 28–150 °C. The device shows a fast response time of 14.3 s even at room temperature. The higher sensitivity of 1% to 11% from 28 to 150 °C was attributed to the presence of the favorable adsorption sites at the edges of MoS₂ flakes. The role of edge sites in hydrogen adsorption is confirmed by partially passivating the edges by depositing the 2–3 nm ZnO film on MoS₂ flakes. This study offers MoS₂ vertically aligned flakes as a promising candidate for the development of fast and low power hydrogen sensors.

See [supplementary materials](#) for growth, photoluminescence, x-ray diffraction, and sensor comparison with other nanostructures.

The authors acknowledge financial support from the Department of atomic energy (DAE) under Project No. 34/20/09/2015/BRNS and also the Department of Physics, IIT Ropar, for providing experimental facility. Jiming Bao acknowledges support from the National Science Foundation (CAREER Award ECCS-1240510) and the Robert A. Welch Foundation (E-1728).

¹J. Hord, *Int. J. Hydrogen Energy* **3**(2), 157 (1978).

²R. F. Cracknell, J. L. Alcock, J. J. Rowson, L. C. Shirvill, and A. Üngüt, "Safety Considerations in Retailing Hydrogen," SAE Technical Paper 2002-01-1928, 2002.

³J.-W. Jiang, *Front. Phys.* **10**(3), 287 (2015).

⁴K. F. Mak, C. Lee, J. Hone, J. Shan, and T. F. Heinz, *Phys. Rev. Lett.* **105**(13), 136805 (2010).

⁵Z. Zhu, J. Yuan, H. Zhou, J. Hu, J. Zhang, C. Wei, F. Yu, S. Chen, Y. Lan, Y. Yang, Y. Wang, C. Niu, Z. Ren, J. Lou, Z. Wang, and J. Bao, *ACS Photonics* **3**(5), 869 (2016).

⁶M.-L. Tsai, S.-H. Su, J.-K. Chang, D.-S. Tsai, C.-H. Chen, C.-I. Wu, L.-J. Li, L.-J. Chen, and J.-H. He, *ACS Nano* **8**(8), 8317 (2014).

⁷C. Liu, D. Kong, P. C. Hsu, H. Yuan, H. W. Lee, Y. Liu, H. Wang, S. Wang, K. Yan, D. Lin, P. A. Maraccini, K. M. Parker, A. B. Boehm, and Y. Cui, *Nat. Nanotechnol.* **11**(12), 1098 (2016).

⁸B. Radisavljevic, A. Radenovic, J. Brivio, V. Giacometti, and A. Kis, *Nat. Nanotechnol.* **6**(3), 147 (2011).

⁹J. Kibsgaard, Z. Chen, B. N. Reinecke, and T. F. Jaramillo, *Nat. Mater.* **11**(11), 963 (2012).

¹⁰S. Y. Cho, S. J. Kim, Y. Lee, J. S. Kim, W. B. Jung, H. W. Yoo, J. Kim, and H. T. Jung, *ACS Nano* **9**(9), 9314 (2015).

¹¹D. J. Late, Y.-K. Huang, B. Liu, Y. Acharya, S. N. Shirodkar, J. Luo, A. Yan, D. Charles, U. V. Waghmare, V. P. Dravid, and C. N. R. Rao, *ACS Nano* **7**(6), 4879 (2013).

¹²C. Kuru, C. Choi, A. Kargar, D. Choi, Y. J. Kim, C. H. Liu, S. Yavuz, and S. Jin, *Adv. Sci.* **2**(4), 1500004 (2015).

¹³Y. Liu, L. Hao, W. Gao, Z. Wu, Y. Lin, G. Li, W. Guo, L. Yu, H. Zeng, J. Zhu, and W. Zhang, *Sens. Actuators, B* **211**, 537 (2015).

¹⁴L. Hao, Y. Liu, W. Gao, Y. Liu, Z. Han, L. Yu, Q. Xue, and J. Zhu, *J. Alloys Compd.* **682**, 29 (2016).

¹⁵M. V. Bollinger, J. V. Lauritsen, K. W. Jacobsen, J. K. Nørskov, S. Helveg, and F. Besenbacher, *Phys. Rev. Lett.* **87**(19), 196803 (2001).

¹⁶T. F. Jaramillo, K. P. Jørgensen, J. Bonde, J. H. Nielsen, S. Horch, and I. Chorkendorff, *Science* **317**(5834), 100 (2007).

¹⁷D. Kong, H. Wang, J. J. Cha, M. Pasta, K. J. Koski, J. Yao, and Y. Cui, *Nano Lett.* **13**(3), 1341 (2013).

¹⁸M. R. Gao, M. K. Y. Chan, and Y. Sun, *Nat. Commun.* **6**, 7493 (2015).

¹⁹H. Wang, Q. Zhang, H. Yao, Z. Liang, H.-W. Lee, P.-C. Hsu, G. Zheng, and Y. Cui, *Nano Lett.* **14**(12), 7138 (2014).

²⁰C. Lee, H. Yan, L. E. Brus, T. F. Heinz, J. Hone, and S. Ryu, *ACS Nano* **4**, 2695 (2010).

²¹A. Splendiani, L. Sun, Y. B. Zhang, T. S. Li, J. Kim, C. Y. Chim, G. Galli, and F. Wang, *Nano Lett.* **10**(4), 1271 (2010).

²²H. L. Skriver and N. M. Rosengaard, *Phys. Rev. B* **46**(11), 7157 (1992).

²³J.-M. Yun, Y.-J. Noh, J.-S. Yeo, Y.-J. Go, S.-I. Na, H.-G. Jeong, J. Kim, S. Lee, S.-S. Kim, H. Y. Koo, T.-W. Kim, and D.-Y. Kim, *J. Mater. Chem. C* **1**(24), 3777 (2013).

²⁴G. Korotcenkov, *Mater. Sci. Eng., B* **139**, 1 (2007).

²⁵I. Sayago, E. Terrado, E. Lafuente, M. C. Horrillo, W. K. Maser, A. M. Benito, R. Navarro, E. P. Urriolabeitia, M. T. Martínez, and J. Gutierrez, *Synth. Met.* **148**(1), 15 (2005).

²⁶D.-H. Baek and J. Kim, *Sens. Actuators, B* **250**, 686 (2017).

²⁷S. Yang, Z. Wang, Y. Zou, X. Luo, X. Pan, X. Zhang, Y. Hu, K. Chen, Z. Huang, S. Wang, K. Zhang, and H. Gu, *Sens. Actuators, B* **248**, 160 (2017).

²⁸J. J. Hassan, M. A. Mahdi, C. W. Chin, H. Abu-Hassan, and Z. Hassan, *Sens. Actuators, B* **176**, 360 (2013).

²⁹X. Liu, T. Xu, X. Wu, Z. Zhang, J. Yu, H. Qiu, J.-H. Hong, C.-H. Jin, J.-X. Li, X.-R. Wang, L.-T. Sun, and W. Guo, *Nat. Commun.* **4**, 1776 (2013).

³⁰Y. Zhou, Y. Liu, W. Zhao, F. Xie, R. Xu, B. Li, X. Zhou, and H. Shen, *J. Mater. Chem. A* **4**(16), 5932 (2016).

³¹M. D. Ganji, N. Sharifi, M. G. Ahangari, and A. Khosravi, *Physica E* **57**, 28 (2014).

³²Q. Yue, Z. Shao, S. Chang, and J. Li, *Nanoscale Res. Lett.* **8**(1), 425 (2013).

³³K. Dolui, I. Rungger, and S. Sanvito, *Phys. Rev. B* **87**(16), 165402 (2013).

³⁴A. Castellanos-Gomez, N. Agrait, and G. Rubio-Bollinger, *Appl. Phys. Lett.* **96**, 213116 (2010).

³⁵M. Kumar, V. N. Singh, F. Singh, K. V. Lakshmi, B. R. Mehta, and J. P. Singh, *Appl. Phys. Lett.* **92**(17), 171907 (2008).

³⁶H. Nan, Z. Wang, W. Wang, Z. Liang, Y. Lu, Q. Chen, D. He, P. Tan, F. Miao, X. Wang, J. Wang, and Z. Ni, *ACS Nano* **8**(6), 5738 (2014).

³⁷S. Ghatak and A. Ghosh, *Appl. Phys. Lett.* **103**(12), 122103 (2013).